EVOLUTION OF INTERNAL WAVES NEAR A TURNING POINT IN THE SOUTH CHINA SEA USING SAR IMAGERY AND NUMERICAL MODELS

Duk-jin Kim[1], David R. Lyzenga[2], Wooyoung Choi[3], and Younsoo Kim[1]

1. Remote Sensing Department, Korea Aerospace Research Institute, Daejeon, 305-333, Korea
2. Naval Architecture and Marine Engineering, University of Michigan, Ann Arbor, MI 48109, USA
3. Department of Mathematical Sciences, New Jersey Institute of Technology, Newark, NJ 07102, USA

ABSTRACT - Subsurface Internal Waves (IWs) can be detected in satellite images as periodic alternating brighter/darker stripes. It is known that there are two types of IWs – depression type and elevation type – depending on the water depth in stratified oceans. In this study, we have quantitatively verified the process of converting polarity from depression waves to elevation waves using ERS-2 SAR images acquired over the northern South China Sea. We simulated the evolution of IWs near a turning point with a numerical model for internal wave propagation. The simulation results near the turning point clearly showed us not only a conversion process of IWs from depression to elevation waves, but also a similar wave pattern with the observed SAR image. We also simulated SAR intensity variation near the turning point. The upper layer currents were computed at regular intervals using the numerical model, as the IWs were passing through the turning point. Then, an integrated hydrodynamic-electromagnetic model was used for simulating SAR intensity profiles from the upper layer currents at each position. The simulated SAR intensity profiles at each position were compared with the observed SAR intensities.

KEY WORDS: Internal Wave, SAR, South China Sea, polarity, numerical model

1. INTRODUCTION

Oceanic internal waves (IWs) can be detected in satellite images as periodic alternating brighter/darker stripes because the local currents induced by the IWs modulate the sea surface capillary and short gravity waves into rougher and smoother zones (Alpers, 1985). It is known that there are two types or polarities of IWs – depression type and elevation type – depending on the water depth and the thermocline depth. Both types of IWs have been observed in synthetic aperture radar (SAR) images (Liu et al., 1998), and the conversion of an IW from one polarity to the other has also been observed using visible (SPOT) imagery (Zhao et al., 2003). In this paper, we present a new SAR observation of this process and a more detailed analysis of the interactions involved. We use a nonlinear internal wave model to predict the surface currents, coupled with a wave action equation to the short surface wave interactions with the internal wave currents and a two-scale radar backscatter model to quantitatively predict the SAR signatures.

2. STUDY AREA AND SAR OBSERVATION

The study area is the northern South China Sea (SCS). It is well known that many IWs are observed in this area and most of them are propagating westward or northwestward. We have focused on the continental shelf area around DongSha Island (Figure 1). One interesting ERS-2 SAR image was taken at 0245 (UTC) on August 22, 2005, as part of the ONR Non-Linear Internal Waves Initiative (NLIWI) project. The SAR image clearly shows IWs propagating west-northwestward. One can also observe that the signature of the first leading IW varies from the lower part to the upper part of the image (Figure 2). While the IW in the lower part of the image shows a narrow bright stripe followed immediately by a broader dark stripe, the IW in the upper part of the image shows that the brighter stripe becomes broader and fades out, and the dark stripe behind it becomes narrower and stronger and is followed immediately by multiple bright and dark stripes. We believe that these variations of IW signature reflect a change in shape and polarity of the IW as it propagates into shallower water.

In general, the polarity of IW (depression or elevation) depends on the water depth relative to the thermocline or mixed layer depth. In the case of depression type of IWs,

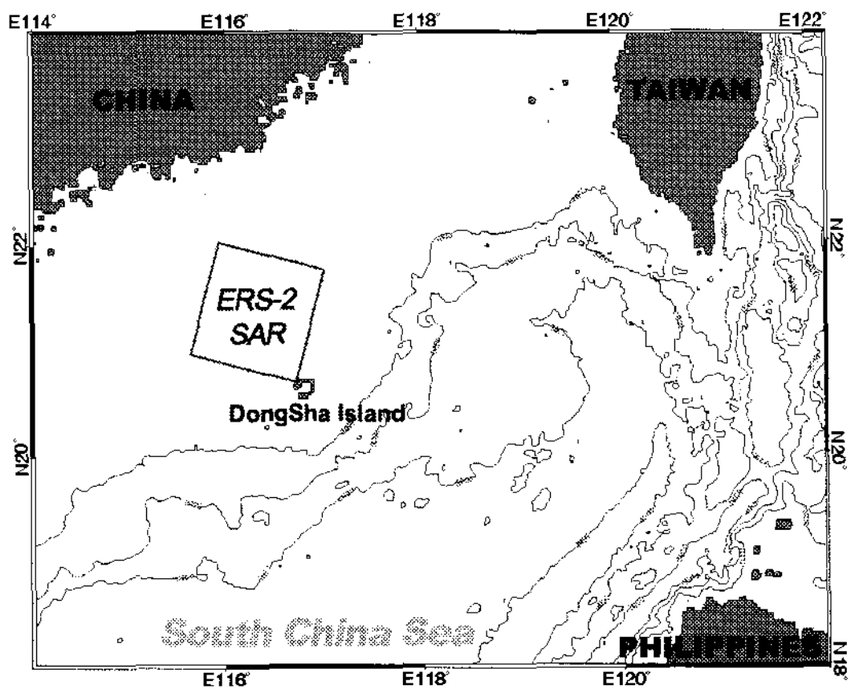

Figure 1. Study area. The ERS-2 SAR coverage area is indicated by the box. Bathymetry map was superimposed on this image. The depth contours were depicted with 1000 m interval.

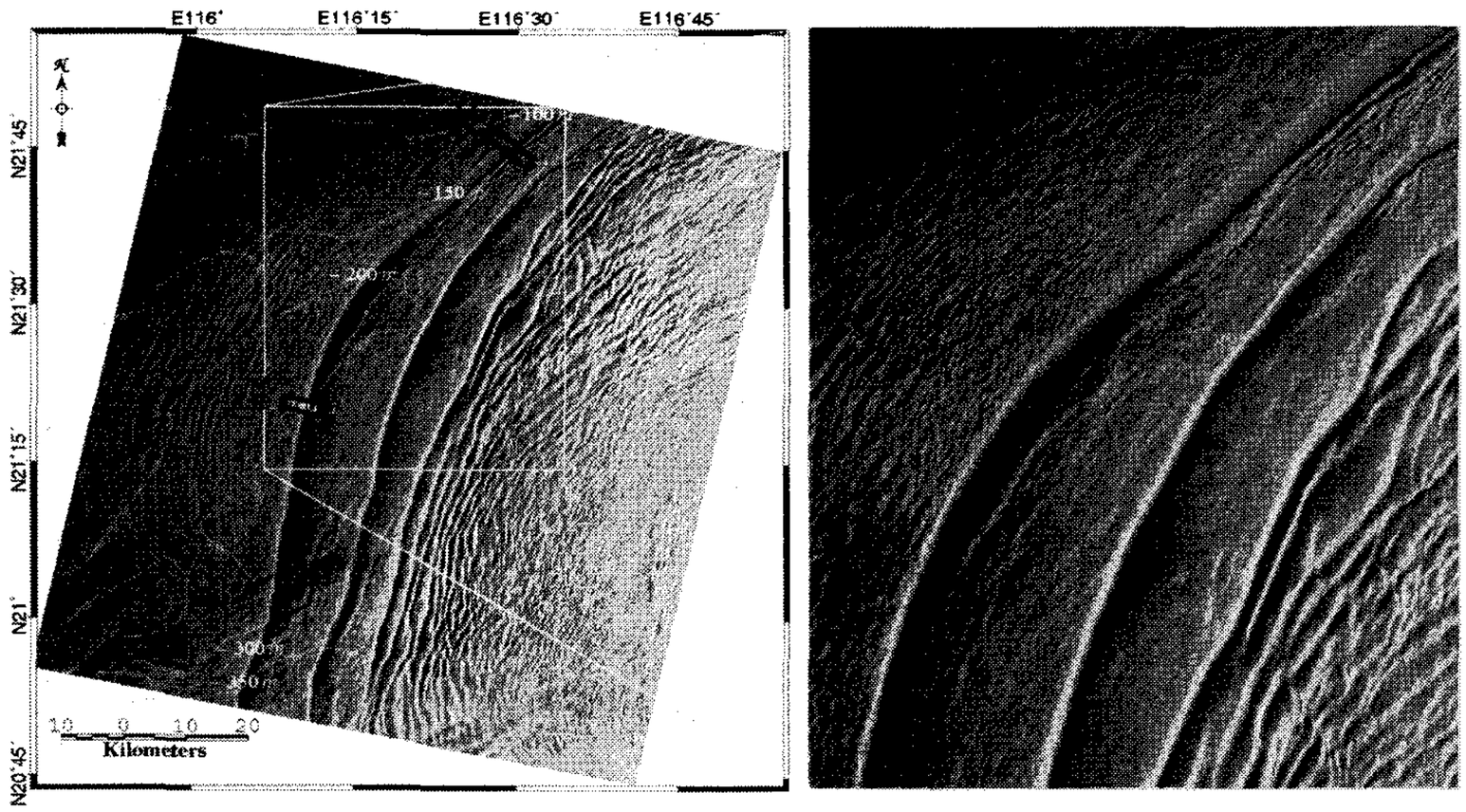

Figure 2. ERS-2 SAR image acquired at 0245 UTC on August 22, 2005.

due to the concave shape of the waveform, the front face slope of the waves is accompanied by downward currents resulting in a convergence zone at the sea surface, while on the rear face there are upward currents resulting in a divergence zone. The interaction of surface waves with these currents cause an increased roughness in the convergence zone and create a brighter stripe in the SAR image, while the smoother surface in the divergent zone creates a darker stripe in the SAR image. In the case of elevation types of IWs, this pattern is reversed, with a darker stripe on the front face and brighter returns on the rear face (Liu et al., 1998). However, these patterns may not always occur, for example in areas where surface slicks or films are abundant such as coastal zones (da Silva et al., 1998). We believe that the IW in the lower part of the image (labeled as A) represents the depression-type IW, and the IW in the upper part of the image (labeled as B) shows evidence of the wave's conversion process from depression to elevation, because the brighter stripe is starting to fade out and a darker stripe followed immediately by a new brighter stripe is starting to appear. The variation of bathymetry in this area also supports this interpretation (Figure 2).

Since the water depth at B is shallower than at A, the IW is expected to change polarity earlier at location A than at location B. Therefore, we can transform the spatial variations of the IW from A to B into the temporal evolution of the IW as it propagates into shallower water. In this study, we have attempted to verify this interpretation by combining numerical models for IW propagation with wave-current interaction and radar backscatter models.

3. SIMULATION OF CONVERSION PROCESS

3.1 Numerical simulation of IW propagation

In order to simulate the propagation and the evolution of IWs over variable bathymetry, we employed a two-layer fluid system with the upper layer depth being constant and the lower layer depth being variable (Figure 3). To make the simulation results applicable to real oceanographic situations, the varying bathymetry corresponding to the study area was taken from the global seafloor topography of Smith and Sandwell (Smith and Sandwell, 1997), and the water densities of the upper and lower layers (ρ_1 and ρ_2) were taken from representative values in the summer season. The initial amplitude of the IW (η_0 at x=86100m) was calculated from the upper and lower layer depths (h_1 and h_2), the density difference ($\Delta\rho$), and the characteristic half width (Δ) by assuming it is in deep water and follows the KdV equation, *i.e.*,

$$\eta_0 = \frac{12\beta}{\alpha\Delta^2} \tag{1}$$

$$c_0 = \left(\frac{g(\rho_2-\rho_1)h_1h_2}{\rho_2h_1+\rho_1h_2}\right)^{1/2} \approx \left(\frac{g\Delta\rho h_1h_2}{\rho_0(h_1+h_2)}\right)^{1/2} \tag{2}$$

$$\alpha = \frac{3c_0}{2h_1h_2}\frac{\rho_2h_1^2-\rho_1h_2^2}{\rho_2h_1+\rho_1h_2} \approx \frac{3c_0(h_1-h_2)}{2h_1h_2} \tag{3}$$

$$\beta = \frac{c_0h_1h_2}{6}\frac{\rho_1h_1+\rho_2h_2}{\rho_2h_1+\rho_1h_2} \approx \frac{c_0h_1h_2}{6} \tag{4}$$

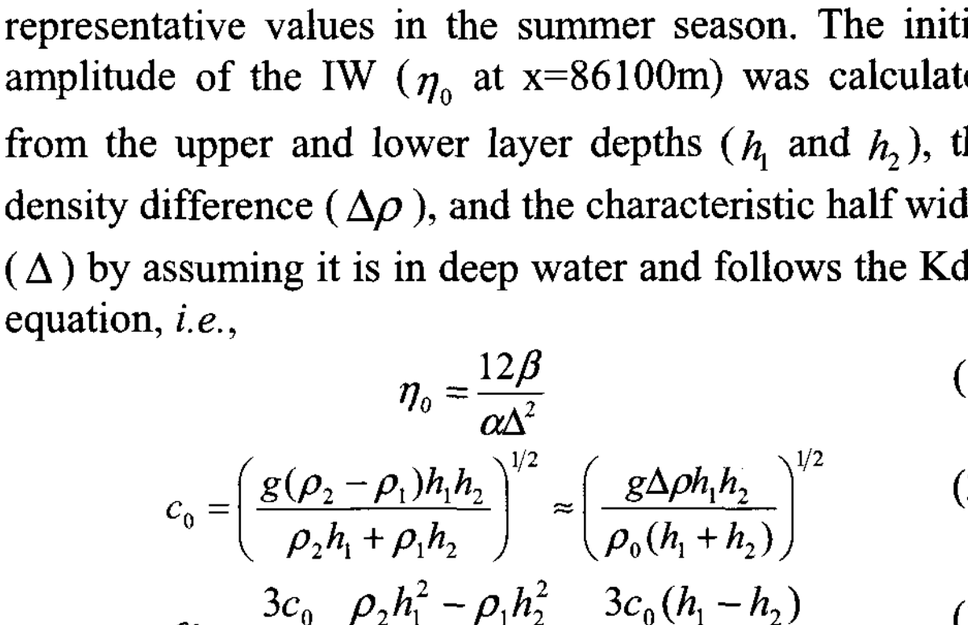

Figure 3. Two-layer fluid system for numerical model simulation.

where, c_0 is the linear phase speed, α and β are coefficients of quadratic nonlinearity and dispersion, respectively. The characteristic half width was estimated from the SAR image through the peak-to-peak method as proposed by Zheng et al. (2001). For the numerical simulation of IW propagation, we used the Lynett and Liu model (Lynett and Liu, 2002). This model was checked with known analytical solutions and, qualitatively, with satellite images taken over the Strait of Gibraltar and near DongSha Island. Figure 4 shows how the IW waveforms evolve as they are passing trough a turning point (which corresponds to the light blue area in Figure 3). One can clearly observe a conversion of the IW from depression to elevation wave. As it propagates westward, the front face slope becomes gentler and broader, and the rear face slope becomes steeper. Elevation waves then start to appear behind the original IW with the rear face of the original depression wave becoming the front face of the newly formed elevation wave. We have extracted the upper layer velocities corresponding to the A and B positions based on the water depth.

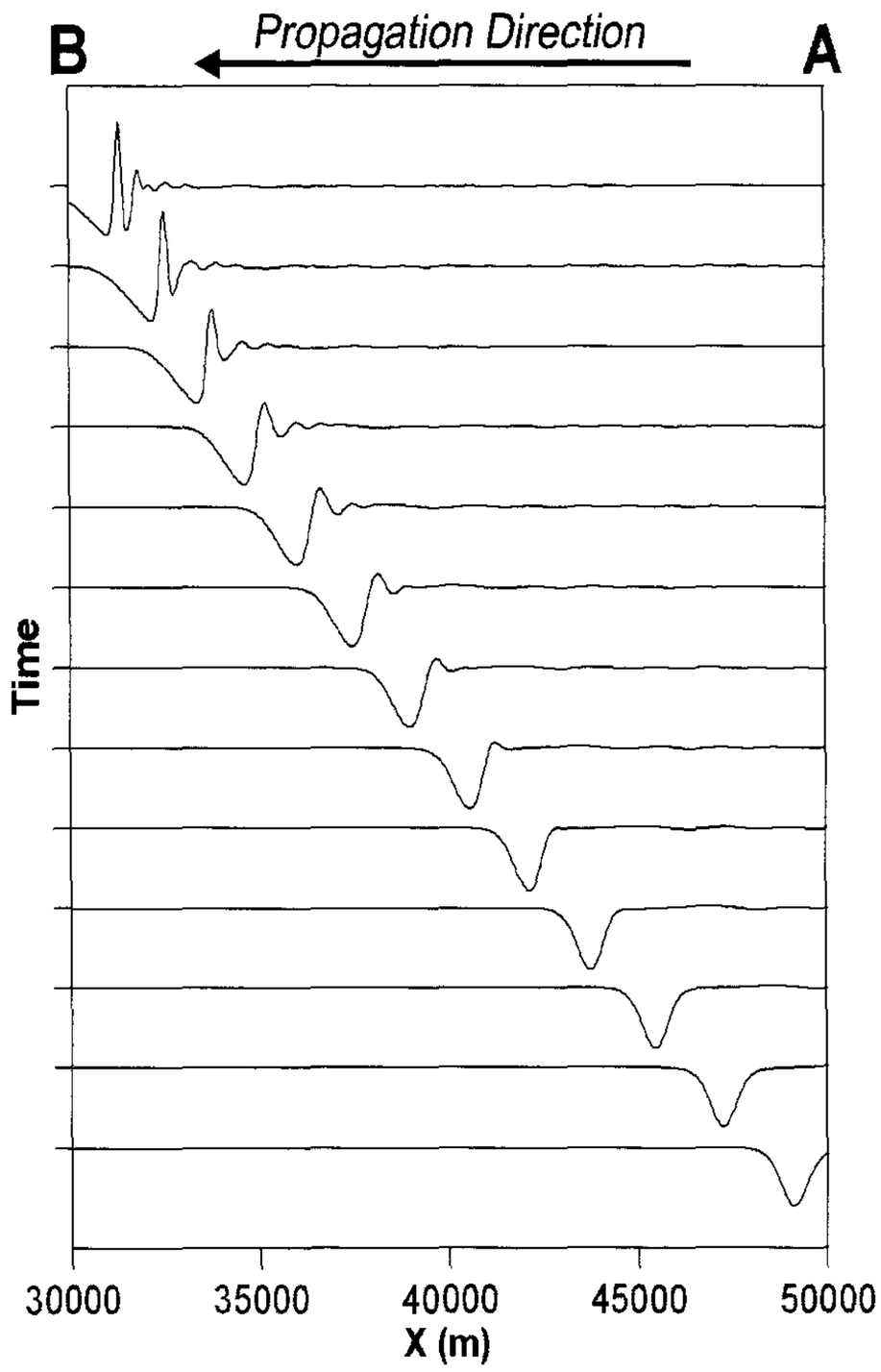

Figure 4. Numerical simulation for IW propagation.

3.2 SAR intensity predictions and comparisons

Having calculated the internal wave currents, we then predicted the SAR intensities using a combined wave-current interaction model and radar backscattering model. The wave-current interaction model is based on the action balance equation

$$\frac{\partial N}{\partial t}+(U+C_g)\frac{\partial N}{\partial x}-\left(k\frac{\partial U}{\partial x}\right)\frac{\partial N}{\partial k}=S(k,x,t) \qquad (5)$$

where N is the action spectral density, C_g is the group velocity, U is the surface current, and k is the wavenumber of the surface waves. The quantity S on the right-hand side of the equation is the net source function which accounts for wind input and wave energy dissipation. The radar backscatter is calculated using the two-scale (tilted Bragg) model. There are several well-known and well-validated models for these purposes. In this study, we adopted the model described in Lyzenga and Bennett (1988) for numerical simulation of SAR imaging.

The wave-current interaction model requires the sea surface wind speed, wind direction and spatially varying surface currents as inputs. The wind speed was estimated from background SAR intensity using a CMOD4 wind retrieval model (Stoffelen and Anderson, 1997), and the wind direction was taken from QuikScat data measured at the nearest time of SAR data acquisition (Remote Sensing Systems). The SAR background intensity (approximately -10dB) corresponds to an estimated wind speed from 2 to 3 m/s depending on the angle of incidence. We have chosen 2.5 m/s as the average wind speed and 45°T as the wind direction. For the spatially varying surface current, we used the depth-averaged horizontal velocities in the upper layer obtained from the numerical model as described in Section 3-1. We also defined a coordinate system for the numerical model prediction, with the x-axis in the direction opposite to the IW propagation direction. The input parameters such as the wind direction and radar look direction were computed relative to this coordinate system. The resulting predicted SAR intensities (Normalized Radar Cross Section; NRCS) from the numerical simulation model are shown in Figure 5 (dotted line). The calculations were performed for C-band VV-polarization (as has the ERS-2 SAR). Improved SAR intensity predictions with a recent ocean wave spectrum (Lyzenga, 2004) derived from CMOD4 model function were also shown in Figure 5 (solid line). This model prediction shows a good agreement with observed background SAR intensity.

For comparison, the observed SAR intensity profiles at A and B positions were shown in Figure 6. Although the magnitudes of predicted modulation are smaller than the observed values from SAR image, the shapes of the predicted modulations agree fairly well with the observations. Therefore, we can confirm that the variation of IWs observed in the ERS-2 SAR image is showing the conversion process from depression to elevation wave, and we could locate the exact position where the upper and lower layer depths are equal (this can be used for estimating the thermocline depth) by transforming the spatial variations of the IW into the temporal evolution of the IW.

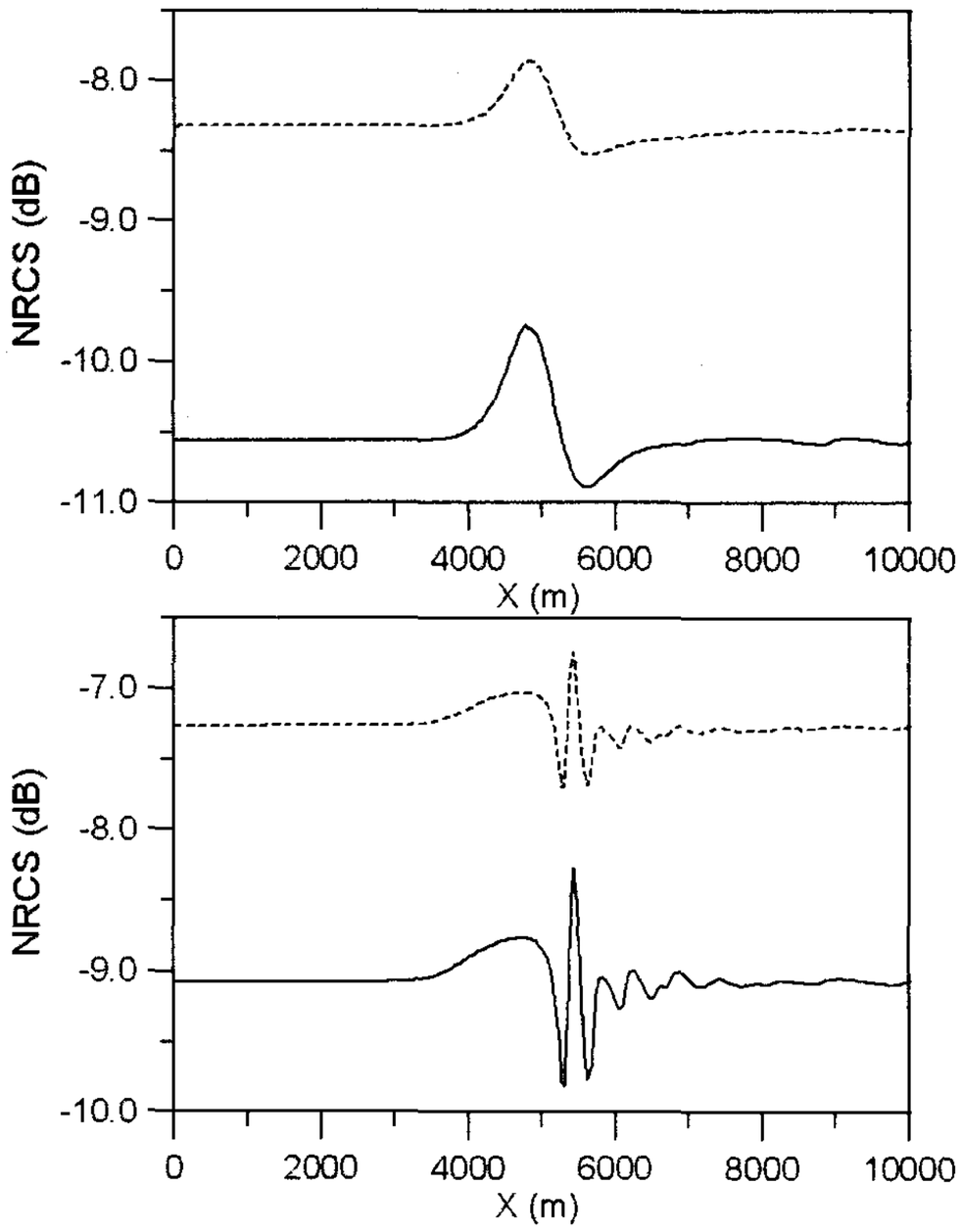

Figure 5. Predicted NRCS at A (upper) and B (lower) positions. Solid lines were predicted with a recent ocean wave spectrum (Lyzenga, 2004).

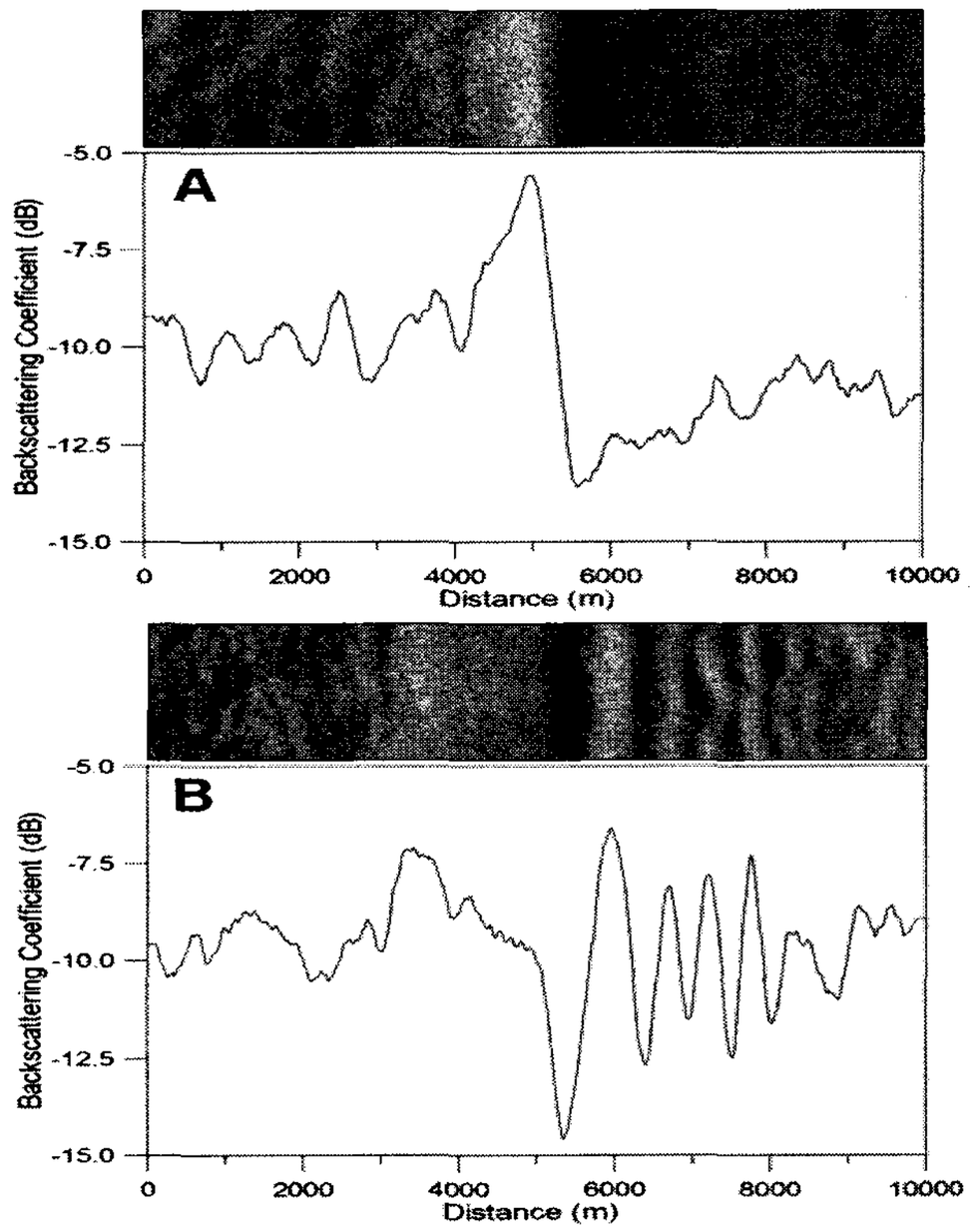

Figure 6. Observed SAR intensities at A (upper) and B (lower) positions.

4. DISCUSSIONS

As shown in Figure 5 and 6, the magnitudes of NRCS modulations predicted from the numerical simulation model are underpredicted. We think the determination of the IW amplitude from the width of SAR intensity variation may not work in this case, because most measurements in the South Chian Sea indicated higher IW amplitudes than we estimated. We also think this is due to the failure to include important terms in the source function of the action balance equation, such as nonlinear wave-wave interactions which transfer energy from longer waves to shorter wavelengths that influence radar backscatter.

REFERENCES

Alpers, W., 1985, Theory of radar imaging of internal waves, *Nature*, 314, pp. 245-247.

da Silva, J.C.B., S.A. Ermakov, I.S. Robinson, D.R.G. Jeans, and S.V. Kijashko, 1998, Role of surface films in ERS SAR signatures of internal waves on the shelf: 1. Short-period internal waves, *J. Geophys. Res.*, 103(c4), pp. 8009-8031.

Liu, A.K., Y.S. Chang, M.-K. Hsu, and N.K. Liang, 1998, Evolution of nonlinear internal waves in the East and South China Seas, *J. Geophys. Res.*, 103(c4), pp. 7995-8008.

Lynett, P.J. and P.L.-F. Liu, 2002, A two-dimensional, depth-integrated model for internal wave propagation over variable bathymetry, *Wave Motion*, 36, pp. 221-240.

Lyzenga, D.R. and J.R. Bennett, 1988, Full-spectrum modeling of synthetic aperture radar internal wave signatures, *J. Geophys. Res.*, 93(c10), pp. 12345-12354.

Lyzenga, D.R., 2004, Ocean wave spectrum and dissipation rate derived from CMOD4 model function, *J. Geophys. Res.*, 109(c07019), doi:10.1029/2003JC002237.

Remote Sensing Systems. [Online]. Available: http://www.ssmi.com/qscat/scatterometer_data_daily.html?rgn=south_east_asia&size=small

Smith W.H.F. and D.T. Sandwell, 1997, Global seafloor topography from satellite altimetry and ship depth soundings, *Science*, 277, pp. 1957-1962.

Stoffelen, A. and D. Anderson, 1997, Scatterometer data interpretation: Estimation and validation of the transfer function CMOD4, *J. Geophys. Res.*, 102(c3), pp. 5767-5780.

Zhao, Z., V.V.Klemas, Q. Zheng, X.-H. Yan, 2003, Satellite observation of internal solitary waves converting polarity," *Geophys. Res. Lett.*, 30(19), doi:10.1029/2003GL018286.

Zheng, Q., Y. Yuan, V. Klemas, and X.-H. Yan, 2001, Theoretical expression for an ocean internal soliton synthetic aperture radar image and determination of the soliton characteristic half width, *J. Geophys. Res.*, 106(c12), pp. 31415-31423.